JACS
JOURNAL OF THE AMERICAN CHEMICAL SOCIETY
Article
pubs.acs.org/JACS

# Intramolecular Electron Transfer in Bipyridinium Disulfides

Gabriel B. Hall,[†] Rudresha Kottani,[†,§] Greg A. N. Felton,[†] Takuhei Yamamoto,[†] Dennis H. Evans,*[,‡] Richard S. Glass,*[,†] and Dennis L. Lichtenberger*[,†]

[†]Department of Chemistry and Biochemistry, The University of Arizona, P.O. Box 210041, Tucson, Arizona 85721, United States
[‡]Department of Chemistry, Purdue University, 560 Oval Drive, West Lafayette, Indiana 47907, United States

Supporting Information

**ABSTRACT:** Reductive cleavage of disulfide bonds is an important step in many biological and chemical processes. Whether cleavage occurs stepwise or concertedly with electron transfer is of interest. Also of interest is whether the disulfide bond is reduced directly by intermolecular electron transfer from an external reducing agent or mediated intramolecularly by internal electron transfer from another redox-active moiety elsewhere within the molecule. The electrochemical reductions of 4,4′-bipyridyl-3,3′-disulfide (**1**) and the di-*N*-methylated derivative ($\mathbf{2}^{2+}$) have been studied in acetonitrile. Simulations of the cyclic voltammograms in combination with DFT (density functional theory) computations provide a consistent model of the reductive processes. Compound **1** undergoes reduction directly at the disulfide moiety with a substantially more negative potential for the first electron than for the second electron, resulting in an overall two-electron reduction and rapid cleavage of the S−S bond to form the dithiolate. In contrast, compound $\mathbf{2}^{2+}$ is reduced at less negative potential than **1** and at the dimethyl bipyridinium moiety rather than at the disulfide moiety. Most interesting, the second reduction of the bipyridinium moiety results in a fast and reversible intramolecular two-electron transfer to reduce the disulfide moiety and form the dithiolate. Thus, the redox-active bipyridinium moiety provides a low energy pathway for reductive cleavage of the S−S bond that avoids the highly negative potential for the first direct electron reduction. Following the intramolecular two-electron transfer and cleavage of the S−S bond the bipyridinium undergoes two additional reversible reductions at more negative potentials.

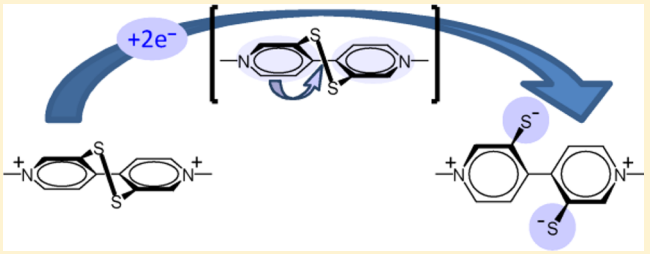


## INTRODUCTION

Electrochemical reduction of compounds with two reducible moieties presents some interesting issues. Is each moiety reduced independently of the other, or is there interaction? This interaction may result from orbital overlap and delocalization of the added electron or by internal electron transfer between orbitals centered on each reducible group.[1,2] This paper examines the electrochemical reduction behavior of disulfides **1** and $\mathbf{2}^{2+}$ (Chart 1). Compounds **1** and $\mathbf{2}^{2+}$ are 1,2-dithiins. The electrochemistry of a number of other 1,2-dithiins has been investigated,[3−8] but those studies have emphasized oxidations, while the current study will focus on the reduction of these compounds and cleavage of the S−S bond. The reductions of **1** and $\mathbf{2}^{2+}$ are of particular interest because they can be viewed as having two sites for reduction: the bipyridine/bipyridinium and disulfide moieties which may interact with each other.

**Chart 1**

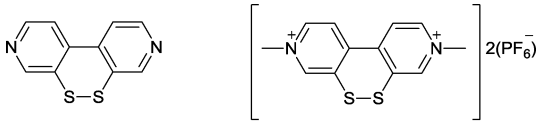


**1** $\mathbf{2}^{2+}$

The electrochemistry of *N*,*N*′-dialkyl-4,4′-bipyridinium salts, viologens, has been extensively investigated because of their importance as herbicides,[9] electron relays,[10] and redox mediators,[11,12] and use in molecular devices.[13,14] Typically they show two low potential reversible one-electron reductions. These potentials depend significantly on the substituents in the bipyridinium rings but not the N-alkyl groups.[15] In geometrically restricted viologens in which there is a bridge of varying length between the 3- and 3′-positions, the dihedral angle between the two planar pyridinium rings roughly correlates with the first reduction potential.[15] Electrochemical reduction of disulfides, especially the mechanism for their reduction, has elicited much interest.[16] Reduction of disulfides is important in biochemistry, and particularly relevant to the studies reported here, biochemical interest in disulfide reduction is stimulated by the important role played by a disulfide anion radical in the mechanism of action of ribonucleotide reductase.[17,18]

We begin with the examination of **1**, whose disulfide bond is preferentially reduced. We find that reduction of the disulfide bond occurs as a two-electron process with potential inversion; that is, the second reduction occurs at a less negative potential

**Received:** January 5, 2014
**Published:** February 14, 2014

   dx.doi.org/10.1021/ja500087m | *J. Am. Chem. Soc.* 2014, 136, 4012−4018

than the first.[19] The result is a two-electron reduction concomitant with disulfide cleavage.

Next we examine $\mathbf{2}^{2+}$, which has both the disulfide bond and bipyridinium as reducible moieties. Recently, it has been reported[20] that a close analogue of $\mathbf{2}^{2+}$, in which the N-substituents of the bipyridinium rings are 4-methyl-benzyl groups, undergoes four reversible one-electron reductions in which two electrons are added to the bipyridinium moiety followed by two-electron reduction of the disulfide moiety to give the ring opened dithiolate. In our studies of the reduction of $\mathbf{2}^{2+}$ by cyclic voltammetry there are four reversible one-electron reductions analogous to the electrochemical results obtained previously, but our results show that the mechanism for these reductions is different from that previously suggested. Specifically we find a fascinating interplay between the redox moieties featuring internal electron transfer from the reduced bipyridinium moiety to the disulfide to cleave the S−S bond at less negative potential than direct reduction of the disulfide.

## RESULTS AND DISCUSSION

**Behavior of 1.** A cyclic voltammogram of **1** in acetonitrile with a glassy carbon electrode is shown in Figure 1. There is a

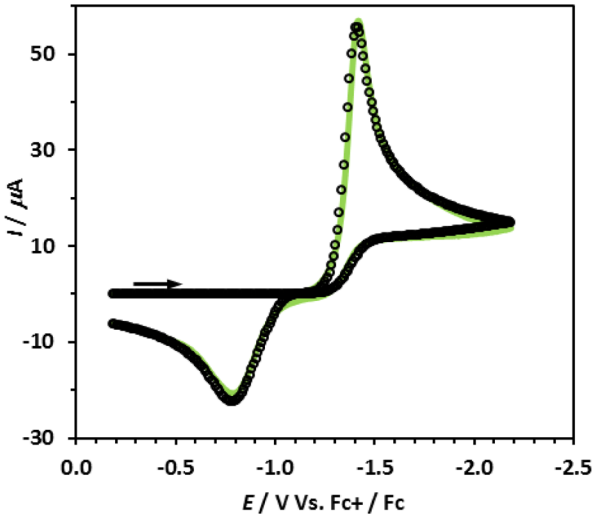


**Figure 1.** Cyclic voltammogram of 0.97 mM **1** in 0.10 M $Bu_4NPF_6$/acetonitrile at 295 K. Glassy carbon working electrode. Scan rate: 0.10 V/s. Green line: background-corrected experimental cyclic voltammogram. Circles: simulation according to reactions 4−5 with the parameter values $E^\circ_4 = -1.35$ V, $\alpha_4 = 0.75$, $k_{s4} = 0.003$ cm/s, $E^\circ_5 = -0.90$ V, $\alpha_5 = 0.66$, $k_{s5} = 0.002$ cm/s; $D_{\text{all species}} = 2.3 \times 10^{-5}$ cm$^2$/s; $r_{\text{disk}} = 0.15$ cm. The simulation is based on diffusion to a disk electrode.

relatively sharp reduction on the initial negative-going scan in the vicinity of −1.4 V versus $Fc^+/Fc$ (ferrocene) and a relatively broad oxidation on the return scan at a considerably more positive potential in the vicinity of −0.8 V. Scans to −2.7 V did not reveal any additional reduction processes. Therefore, rather than two single electron reductions of the disulfide bond at separated potentials, the two-electron reduction of the disulfide bond is encompassed in the reduction around −1.4 V. The reductive current is also consistent with two-electron processes in our system and further supported by simulations and computations discussed later. A chemical process must also take place such that the return oxidation does not occur until a much more positive potential, where again a two-electron process takes place. Subsequent scans reproduce the CV (cyclic voltammogram) trace in Figure 1, showing the overall chemical reversibility of the reduction followed by the oxidation process.

The mechanism commonly used for explanation of the reduction of the disulfide bond is an initial one-electron reduction to the radical anion followed by a rapid cleavage of the S−S bond to a $S^\bullet$ radical and $S^-$ anion, and then reduction of the $S^\bullet$ radical with a second electron to a second $S^-$ anion.[21−23] This mechanism is depicted for molecule **1** with the three steps shown in Scheme 1. However, it was suggested

**Scheme 1**

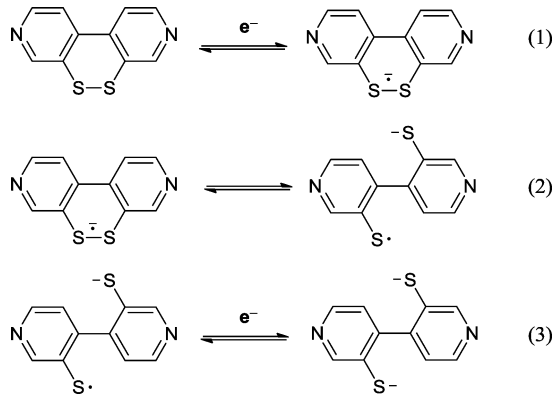


that in the reduction of the cyclic disulfide dibenzo-1,2-dithiin cleavage of the disulfide bond occurs after the addition of the second electron, and addition of the second electron has a less negative potential than addition of the first electron (potential inversion).[24,25]

The cyclic voltammograms of **1** at several scan rates were simulated with the mechanism shown in Scheme 1, and the simulations are illustrated in the Supporting Information in Figure S1. Note that the potential for step 1 of −1.44 V versus $Fc^+/Fc$ is considerably more negative than the potential for step 3 of −0.89 V, so the system demonstrates a less negative potential for the second than the first reduction (potential inversion). An important feature of the simulation is that the S−S bond cleavage and rotation in step 2 of Scheme 1 must be rapid on the electrochemical time scale so that both two-electron reduction on the negative-going scan and two-electron oxidation on the return scan are observed. This requirement is a challenge for simulations of CVs obtained at fast scan rates as discussed below.

Further insight into the addition of the first electron to **1** and the driving force for addition of the second electron is obtained from the computational results. The LUMO calculated for **1** is shown in Figure 2. It shows a mixture of aromatic ring character and antibonding character between the sulfur atoms which would promote S−S bond cleavage with electron occupation by reduction. There is some bonding interaction between the 4 and 4′ carbons in the LUMO of molecule **1**, but when the LUMO is occupied to form the anion this bonding interaction is much reduced, as seen in the SOMO of $\mathbf{1}^-$ in Figure 2. Thus, the first electron upon reduction goes into an orbital dominated by S−S antibonding character, causing $\mathbf{1}^-$ to lengthen the S−S distance and correspondingly open the S−C4−C4′−S′ torsion angle from ∼30° to ∼40° for geometries optimized with acetonitrile solvation (Figure 3). This results in the SOMO consisting of almost exclusively S−S antibonding character and virtually no C4−C4′ $\pi$ bonding character. The potential


dx.doi.org/10.1021/ja500087m | J. Am. Chem. Soc. 2014, 136, 4012−4018

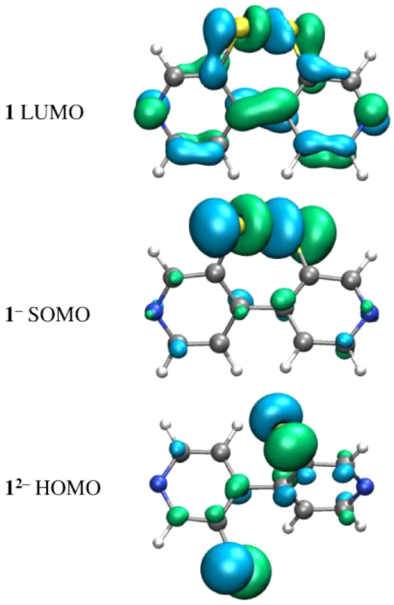


**Figure 2.** Reduction-active orbital of **1** occupied with 0, 1, and 2 electrons, top to bottom, respectively. Top is the LUMO (lowest unoccupied molecular orbital) of **1**, middle is the SOMO (singly occupied molecular orbital) of $\mathbf{1}^{-}$, and bottom is the HOMO (highest occupied molecular orbital) of $\mathbf{1}^{2-}$ (isosurface values ±0.05).

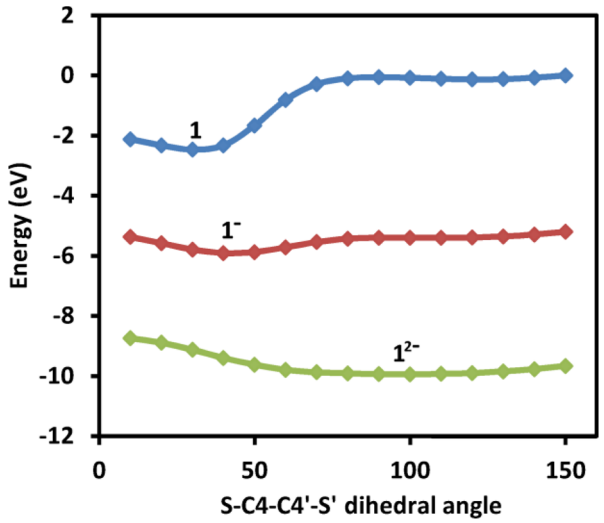


**Figure 3.** Energy rotation profile, with respect to the S−C4−C4′−S′ torsion angle for all of the oxidation states of **1**.

calculated for the first reduction step is −1.35 V versus $Fc^{+}/Fc$ in acetonitrile.

The potential energy as a function of the breaking of the S−S bond and concomitant rotation about the S−C4−C4′−S′ torsion angle is shown in Figure 3. A second shallow well for $\mathbf{1}^{-}$ is present 0.51 eV higher in energy at a torsion angle of ∼100° with the sulfur atoms rotated away from each other. This calculated S−S bond energy in the anion is reasonable considering that the first reduction lowers the formal S−S bond order from one in the neutral molecule to one-half in the anion. However, this energy poses a problem for the mechanism in Scheme 1, where the S−S bond breaking process in step 2 must be thermodynamically favorable and fast in comparison to the first electron transfer rate in order to reasonably account for the two-electron reduction step in the CV shown in Figure 1.

Explanation of the voltammogram lies in consideration of the second reduction. There are two important results from the computations with regard to the CV in Figure 1. First the second reduction potential is calculated to be −0.76 V. In comparison to the calculated first reduction potential of −1.35 V, this represents a case where the second reduction occurs at a substantially less negative potential, such that when the neutral molecule is reduced to the anion at −1.35 V there is a strong driving force for the second reduction to the dianion. The second reduction occurring at a significantly less negative potential than the first also accounts for the wide separation between the reduction and return oxidation peaks. Second, the potential energy curve in Figure 3 shows that upon reduction to $\mathbf{1}^{2-}$ the S−S bond breaks, and the sulfur atoms rotate away from each other to a S−C4−C4′−S′ torsion angle of ∼100° with no calculated barrier to rotation. Thus, due to the second reduction occurring at a less negative potential, the anion radical of **1** rapidly reduces to the dianion, and cleavage of the S−S bond is concerted with the *second* reduction.

The return oxidation scan is understood similarly. When the dianion is oxidized to the anion there is a strong driving force (on the order of 0.5 V) for oxidizing the anion to the neutral molecule and reforming the S−S bond.

Thus, the potential curves suggest an alternative mechanism to account for the CV in Figure 1, shown in Scheme 2, in which

**Scheme 2**

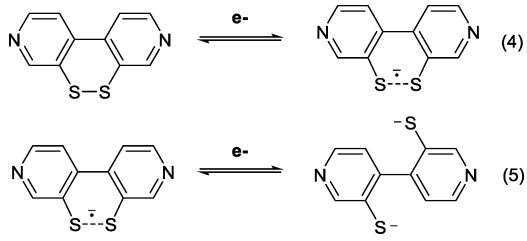


the S−S bond is elongated upon initial reduction to $\mathbf{1}^{-}$ and cleavage of the S−S bond occurs with the second reduction. Simulations of the experimental voltammograms using this simple mechanism produced good fits over a wide range of scan rates. The simulation at 0.10 V/s is shown in Figure 1, and the simulations at other scan rates are shown in the Supporting Information (Figure S1). The reduction potentials in these simulations of −1.35 and −0.90 V are in good agreement with the computational values of −1.35 and −0.79 V. Other mechanisms and simulation parameters are possible, but the simulation parameters and mechanism presented in Scheme 2 are consistent with the computations and the experimental CV. In spite of fewer adjustable parameters in the simulations with Scheme 2 than in Scheme 1, the simulations are overall more successful with Scheme 2. Regardless of the exact mechanism, the important point for the following discussion is recognition of the strong driving force for cleavage of the S−S bond with the second electron reduction.

**Behavior of $\mathbf{2}^{2+}$.** The cyclic voltammogram obtained for $\mathbf{2}^{2+}$ is shown in Figure 4. Two pairs of voltammetric peaks are seen, with the first pair strongly overlapping between −0.4 and −0.6 V. Note that the first pair of reductions occurs at potentials less negative than those found for **1**, as one might expect from imparting a formal positive charge on the pyridinium rings. In


dx.doi.org/10.1021/ja500087m | J. Am. Chem. Soc. 2014, 136, 4012−4018

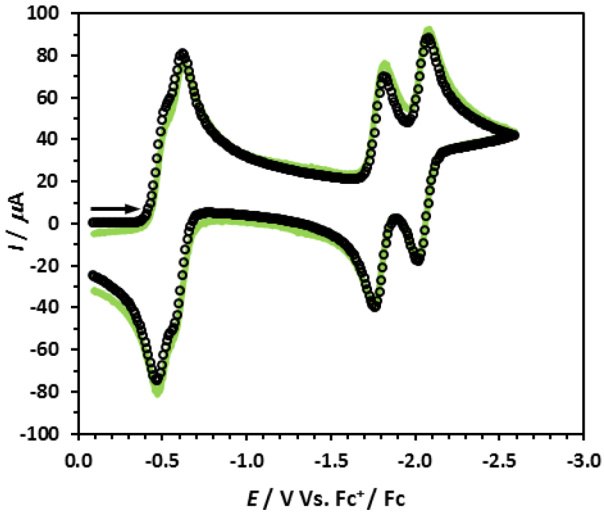


**Figure 4.** Cyclic voltammogram of 0.73 mM $2^{2+}$ in 0.10 M n-$Bu_4NPF_6$/acetonitrile at 298 K. Glassy carbon working electrode. Scan rate: 1.00 V/s. Green line: background-corrected experimental cyclic voltammogram. Circles: simulation for four successive reversible electron−transfer reactions. The reactions were treated as reversible ($k_s$ values set at 0.3 cm/s). Standard potentials: $E^\circ_1 = -0.49$; $E^\circ_2 = -0.60$; $E^\circ_3 = -1.79$; $E^\circ_4 = -2.05$ V. $D_{\text{all species}} = 1.9 \times 10^{-5}$ cm$^2$/s.

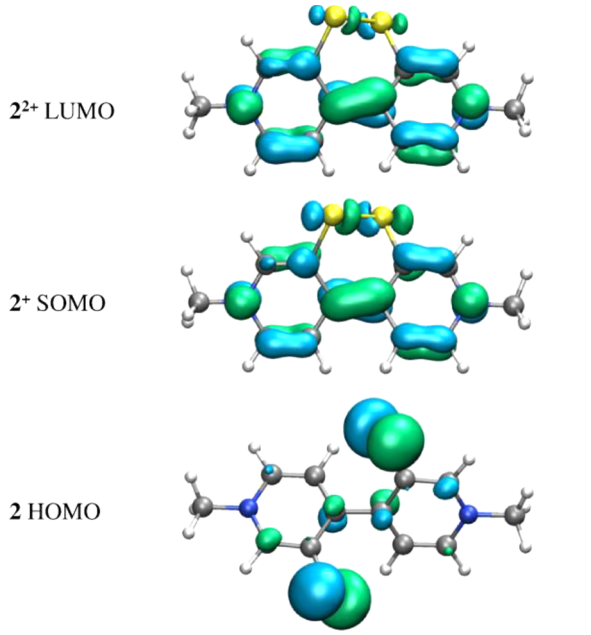


**Figure 5.** Reduction-active orbital of **2** occupied with 0, 1, and 2 electrons, top to bottom, respectively. Top is the LUMO of $2^{2+}$, middle is the SOMO of $2^+$, and bottom is the HOMO of **2** (isosurface values ±0.05).

addition, these processes are fully chemically reversible on the voltammetric time scale as attested to by the good fit of the simulation with the experimental voltammogram. One also notes the second pair of reversible reduction processes in the region −1.7 to −2.0 V. The reduction potentials of bipyridinium salts depend on the dihedral angle between the two heterocyclic rings, with increasing planarity between the two rings making reduction more facile. In the solid state, this angle is 32° for **1**,[20] which closely matches our computed gas-phase value of 34°. This is also close to the computed value for $2^{2+}$ of 36° and is considerably less than that for gas-phase computed methyl viologen$^{2+}$ (44°)[26,27] On reduction, the dihedral angle is calculated to be close to 0° for the methyl viologen cation, promoting electron delocalization between the two rings. Consequently reduction of $2^{2+}$ should be more facile than methyl viologen$^{2+}$, and there is also a substituent effect on the reduction potentials for $2^{2+}$. Indeed the first two reduction potentials for $2^{2+}$ are less negative than the corresponding standard potentials for methyl viologen$^{2+}$ of −0.80 and −1.25 V.[28] The standard potentials for the four steps of reduction of $2^{2+}$ are −0.49, −0.60, −1.79, and −2.05 V, which compare favorably with the DFT calculated values of −0.55, −0.64, −1.75, and −2.16 V. An important note that comes up later is that, unlike **1**, subsequent reductions occurring at less negative potentials than prior reductions is not evidenced experimentally or indicated computationally.

The positive charges in the pyridinium rings of $2^{2+}$ result in a calculated LUMO, shown in Figure 5, consisting mostly of heterocyclic ring $\pi$-character with minimal S−S antibonding character. This suggests that upon reduction the first electron will go into an orbital consisting almost entirely of the bipyridinium $\pi$-system and not a mixed orbital with considerable S−S antibonding character as was the case with **1**.

This is comparable to that suggested for the reduction of bis-*p*-nitrophenyl disulfide,[23,29,30] where two energy minima were computationally identified: one with the unpaired electron localized on a nitro group with only a slightly elongated S−S bond and the other localized on the S−S bond with an elongated S−S bond similar to other disulfide anion radicals.

DFT calculations show the SOMO of $2^+$ is primarily composed of pyridinium $\pi$-character with the S−S bond intact, having almost identical orbital contributions as the LUMO of $2^{2+}$; i.e., almost no change in orbital character takes place upon the first reduction as seen from Figure 5. According to the computations the optimal S−S bond distance in the dication lengthens only 0.05 Å with the first reduction of the molecule, whereas for molecule **1** the lengthening is 0.55 Å with the first reduction.With the SOMO of $2^+$ being the orbital for the next reduction, initial insertion of an electron to form **2** is into the pyridinium $\pi$-system. The orbital energy gap in $2^+$ to the next highest orbital is 1.3 eV, indicating the strong preference of the positively charged bipyridinium unit to accept the electron over the S−S antibonding orbital in the geometry of $2^+$. However, with acceptance of the electron to form neutral **2**, the strong driving force for two-electron cleavage of the S−S bond takes hold (Figure 6). An internal two-electron transfer occurs from the $\pi$-system to the S−S antibond, causing complete cleavage of the S−S bond and rotation of the bipyridinium rings about the C4−C4′ bond to separate the charged atoms and minimize the electron−electron repulsions.

The internal electron transfer and concomitant geometric rearrangement yields a HOMO of **2** (Figure 5) almost entirely sulfur in character leaving the aromatic bipyridinium rings free to accept additional electrons (see the LUMO of **2** in Figure 7). The separated two-step reduction of **2** to $2^{2-}$ involves addition of electrons to the newly vacated $\pi$ bipyridinium orbitals, and DFT computations show that they are composed of much the same character as those involved in the reduction from $2^{2+}$ to **2** (compare Figures 5 and 7). However, with the S−S bond already cleaved to form the dithiolate and no internal electron transfer possible, there is no major geometric rearrangement upon further reduction to the anion and dianion.


dx.doi.org/10.1021/ja500087m | J. Am. Chem. Soc. 2014, 136, 4012−4018

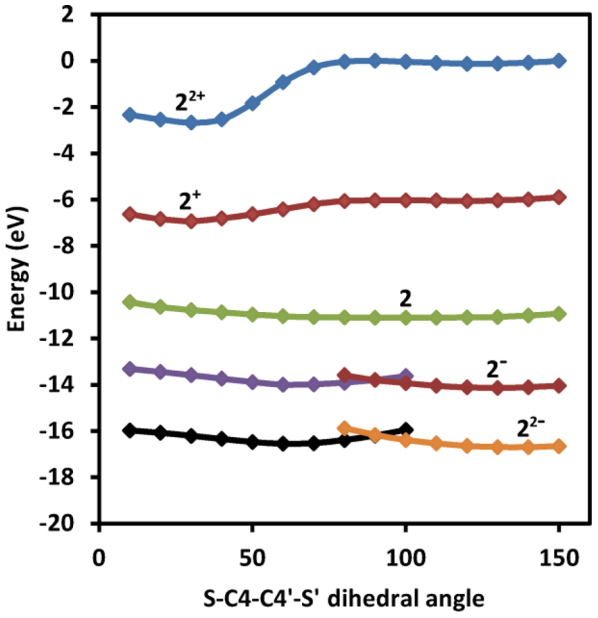


**Figure 6.** Energy rotation profile, with respect to the S−C4−C4′−S′ torsion angle for all of the oxidation states of **2**.

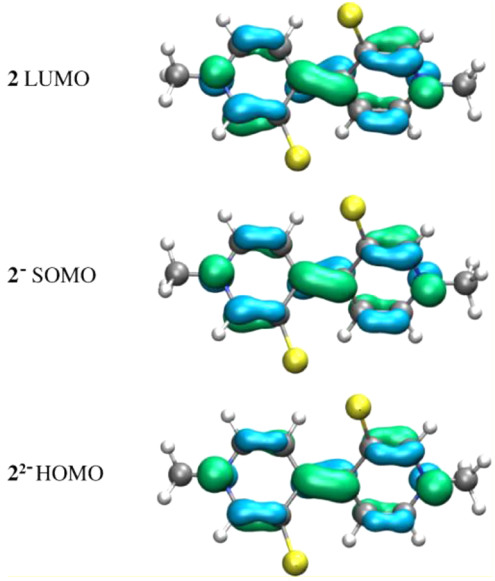


**Figure 7.** Reduction-active orbital of **2** occupied with 2, 3, and 4 electrons, top to bottom, respectively. Top is the LUMO of **2**, middle is the SOMO of $\mathbf{2}^{-}$, and bottom is the HOMO of $\mathbf{2}^{2-}$ (isosurface values ±0.05).

On the return scan, $\mathbf{2}^{2-}$ undergoes two one-electron oxidations with removal of the electrons coming from the reduced aromatic system. Oxidation of **2** to $\mathbf{2}^{+}$ is accompanied by reformation of the disulfide bond and intramolecular transfer of the other disulfide electron back to the bipyridinium, such that the last step of the oxidation scan, $\mathbf{2}^{+}$ to $\mathbf{2}^{2+}$, is the reverse of the initial bipyridinium-centered reduction.

In spite of the reversible processes seen in cyclic voltammetry, some slow chemical reactions occur with longer time scale studies. Controlled potential electrolysis was conducted on $\mathbf{2}^{2+}$ with the aim of generating a solution of $\mathbf{2}^{+}$. More than one Faraday of charge was required per mole of the disulfide to achieve complete electrolysis. When electrolysis was interrupted after passage of one Faraday per mole, voltammetric investigation of the blue electrolysis solution was not consistent with the presence of the radical cation, $\mathbf{2}^{+}$, but indicated the presence of other unknown products.

Additionally, mono-*N*-methyl-4,4′-bipyridyl-3,3′-disulfide ($\mathbf{3}^{+}$) was synthesized and investigated electrochemically (Supporting Information Figure S5). This monomethylated derivative is a step between compound **1** and the dimethylated compound $\mathbf{2}^{2+}$, and showed behavior intermediate between **1** and $\mathbf{2}^{2+}$. In this case the first two reductions appear to be at similar potential with the addition of the second electron apparently at slightly less negative potential than the first, and a third reduction is well separated from the first two at more negative potential. However, the compound was found to precipitate onto the electrode in the course of the CV scan making detailed modeling of the experimental results impractical. Additional information can be found in the Supporting Information.

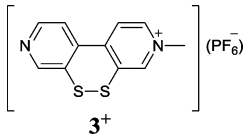


$\mathbf{3}^{+}$

## CONCLUSIONS

The difference between the present model of the reductions of these complexes and the previous studies lies in the interpretation of the S−S bond breaking mechanism. Previous work describes a "loose radical-ion dissociative ET (electron transfer) mechanism" in which the disulfide radical anion irreversibly dissociates to a sulfur-based radical and a sulfur-based anion.[1,30] The sulfur-based radical is then "eventually" reduced to a second sulfur-based anion giving "an overall two-electron process".[29] However, this mechanism does not lead to a satisfactory simulation of the cyclic voltammograms of the disulfide molecules in this study over a wide range of scan rates. The computations presented here indicate that S−S bond breaking from the disulfide radical anion is not favored. Instead, there is a strong driving force for breaking of the S−S bond with acceptance of the second electron. The second electron, rather than simply reducing a radical fragment product of a prior S−S bond dissociation, instead is utilized to drive the S−S bond dissociation in a second step from the disulfide radical anion.

In summary, we see considerably different behavior upon reduction of disulfides **1** and $\mathbf{2}^{2+}$, and the empirical electrochemical results are modeled and explained well with simulations and DFT computations. For **1**, addition of the first electron to the disulfide moiety requires considerably higher negative potential than addition of the second electron, which at that point is accompanied by rapid rupture of the S−S bond forming the ring-opened dithiolate. For $\mathbf{2}^{2+}$, two one-electron reductions of the bipyridinium moiety occur at less negative potential than the reductions of **1** and proceed to an intramolecular two-electron charge transfer to open to the dithiolate. Most significant, the redox-active bipyridinium moiety provides a lower energy route to cleavage of the S−S bond that avoids the high negative potential for the first direct electron reduction of the disulfide. After transfer of two electrons to the disulfide, the bipyridinium ring can once again be twice reduced. DFT computations show that all of the annulated compounds retain some S−S bond order with single


dx.doi.org/10.1021/ja500087m | *J. Am. Chem. Soc.* 2014, 136, 4012−4018

electron reduction, but with the second electron reduction all proceed without barrier to the broken S−S bond, as might be expected for the formal S−S bond order of zero following two-electron reduction and the charge repulsion between the two negatively charged thiolates that result.

## EXPERIMENTAL SECTION

Synthesis and characterization of **1** has been reported[20] elsewhere. Synthesis of $\mathbf{2}^{2+}$ will be reported in a separate manuscript, but is very similar to the synthesis of the known bipyridinium disulfide.[20] Sources and treatment of solvent and electrolyte were the same as reported earlier.[31] Electrochemical procedures including the determination and compensation of solution resistance have also been reported.[31] The working electrode was a 0.3-cm diameter glassy carbon disk whose area was calibrated by studies of the oxidation of ferrocene in acetonitrile at 298 K using $2.5 \times 10^{-5}$ $cm^2/s$ as the diffusion coefficient of ferrocene.[32] The laboratory reference electrode was a silver wire in contact with 0.010 M $AgNO_3$ in acetonitrile which also contained 0.10 M n-$Bu_4NPF_6$. Periodically the reversible potential for the ferrocenium/ferrocene couple, $Fc^+/Fc$, in acetonitrile was determined with respect to the silver reference electrode, which allowed for post facto expression of all reported potentials versus ferrocene. Simulations were carried out using DigiElch[33] (http://www.elchsoft.com) with either planar or disk geometry for the working electrode.

All computations were performed using the Amsterdam Density Functional Theory program version adf2013.01.[34−36] Computations were carried out with the PBE functional[37] with dispersion corrections according to the method of Grimme using the BJ damping function (PBE-D3-BJ).[38] The effect of different basis sets was explored, and the reported results utilize a double-$\zeta$ valence (DZ) for hydrogen atoms and triple-$\zeta$ plus polarization (TZP) for all other atoms. Relativistic effects are included by the zero order regular approximation[39] (ZORA). Solvation free energies are estimated by the conductor-like screening model[40] (COSMO) of solvation using default parameters for acetonitrile. It was found necessary to carry out all geometry optimizations in solvent because stabilization of the positively and negatively charged species in acetonitrile had noticeable effects on the potential energy surfaces. Calculations of the reduction potentials included the electronic energies in solvent, the zero-point vibrational energies unscaled from harmonic frequency calculations, and thermal enthalpy and entropy contributions in solution at 298.15 K. The solution translational and rotational entropy was estimated as described before,[41] but regardless of the definition has little effect on the calculated potential. Figures of the optimized geometries and molecular orbitals were created with program Visual Molecular Dynamics.[42]

## ASSOCIATED CONTENT

### Supporting Information

Simulations of the cyclic voltammograms of **1** at different scan rates, scan rate study of **1** with normalized current, a text file of all computed molecule Cartesian coordinates in .xyz format for convenient visualization, example keywords of the computations, and computational and electrochemical data for mono-*N*-methyl-4,4′-bipyridyl-3,3′-disulfide. This material is available free of charge via the Internet at http://pubs.acs.org.

## AUTHOR INFORMATION


### Corresponding Authors

evansd@purdue.edu
rglass@email.arizona.edu
dlichten@email.arizona.edu

### Present Address

[§]Organix Inc., 240 Salem Street, Woburn, MA 01801.


### Author Contributions

The manuscript was written through contributions of all authors.

### Notes

The authors declare no competing financial interest.

## ACKNOWLEDGMENTS

The support of the National Science Foundation through the Collaborative Research in Chemistry program, Grants CHE 0527003 and 1111718, is gratefully acknowledged.

## REFERENCES


(1) Antonello, S.; Maran, F. *Chem. Soc. Rev.* **2005**, *34*, 418.
(2) Houmam, A. *Chem. Rev.* **2008**, *108*, 2180.
(3) Wakamiya, A.; Nishinaga, T.; Komatsu, K. *J. Am. Chem. Soc.* **2002**, *124*, 15038.
(4) Block, E.; Birringer, M.; DeOrazio, R.; Fabian, J.; Glass, R. S.; Guo, C.; He, C.; Lorance, E.; Qian, Q.; Schroeder, T. B.; Shan, Z.; Thiruvazhi, M.; Wilson, G. S.; Zhang, X. *J. Am. Chem. Soc.* **2000**, *122*, 5052.
(5) Zhu-Ohlbach, Q.; Gleiter, R.; Rominger, F.; Schmidt, H.-L.; Reda, T. *Eur. J. Org. Chem.* **1998**, 2409.
(6) Schroth, W.; Dunger, S.; Billig, F.; Spitzner, R.; Herzschuh, R.; Vogt, A.; Jende, T.; Israel, G.; Barche, J.; Ströhl, D.; Sieler, J. *Tetrahedron* **1996**, *52*, 12677.
(7) Dakova, B.; Carbonnelle, P.; Walcarius, A.; Lamberts, L.; Evers, M. *Electrochim. Acta* **1992**, *37*, 725.
(8) Hennig, H.; Schumer, F.; Reinhold, J.; Kaden, H.; Oelssner, W.; Schroth, W.; Spitzner, R.; Hartl, F. *J. Phys. Chem. A* **2006**, *110*, 2039.
(9) Summers, L. A. *The Bipyridinium Herbicides*; Academic Press: New York, 1980.
(10) Nada, A. A.; Hamed, H. A.; Barakat, M. H.; Mohamed, N. R.; Veziroglu, T. N. *Int. J. Hydrogen Energy* **2008**, *33*, 3264.
(11) Ghica, M. E.; Brett, C. M. A. *Anal. Chim. Acta* **2005**, *532*, 145.
(12) Aulenta, F.; Canosa, A.; Majone, M.; Panero, S.; Reale, P.; Rossetti, S. *Environ. Sci. Technol.* **2008**, *42*, 6185.
(13) Saha, S.; Stoddart, J. F. *Chem. Soc. Rev.* **2007**, *36*, 77.
(14) Andersson, S.; Zou, D.; Zhang, R.; Sun, S.; Aakermark, B.; Sun, L. *Eur. J. Org. Chem.* **2009**, 1163.
(15) Benniston, A. C.; Harriman, A.; Li, P.; Rostron, J. P.; Harrington, R. W.; Clegg, W. *Chem.—Eur. J.* **2007**, *13*, 7838.
(16) Glass, R. S. In *Organic Electrochemistry*, 5th ed.; Hammerich, O., Speiser, B., Eds.; Taylor & Francis: London; Chapter 9.
(17) Lawrence, C. C.; Bennati, M.; Obias, H. V.; Bar, G.; Griffin, R. G.; Stubbe, J. *Proc. Natl. Acad. Sci. U.S.A.* **1999**, *96*, 8979.
(18) Lenz, R.; Giese, B. *J. Am. Chem. Soc.* **1997**, *119*, 2784.
(19) Evans, D. H. *Chem. Rev.* **2008**, *108*, 2113.
(20) Benniston, A. C.; Hagon, J.; He, X.; Yang, S.; Harrington, R. W. *Org. Lett.* **2012**, *14*, 506.
(21) Maran, F.; Wayner, D. D. M.; Workentin, M. S. *Adv. Phys. Org. Chem.* **2001**, *36*, 85.
(22) Antonello, S.; Benassi, R.; Gavioli, G.; Taddei, F.; Maran, F. *J. Am. Chem. Soc.* **2002**, *124*, 7529.
(23) Antonello, S.; Daasbjerg, K.; Jensen, H.; Taddei, F.; Maran, F. *J. Am. Chem. Soc.* **2003**, *125*, 14905.
(24) Benniston, A. C.; Allen, B. D.; Harriman, A.; Llarena, I.; Rostron, J. P.; Stewart, B. *New J. Chem.* **2009**, *33*, 417.
(25) Llarena, I.; Benniston, A. C.; Izzet, G.; Rewinska, D. B.; Harrington, R. W.; Clegg, W. *Tetrahedron Lett.* **2006**, *47*, 9135.
(26) Castellà-Ventura, M.; Kassab, E. *J. Raman Spectrosc.* **1998**, *29*, 511.
(27) Ould-Moussa, L.; Poizat, O.; Castella-Ventura, M.; Buntinx, G.; Kassab, E. *J. Phys. Chem.* **1996**, *100*, 2072.
(28) Braterman, P. S.; Song, J. I. *J. Org. Chem.* **1991**, *56*, 4678.
(29) Daasbjerg, K.; Jensen, H.; Benassi, R.; Taddei, F.; Antonello, S.; Gennaro, A.; Maran, F. *J. Am. Chem. Soc.* **1999**, *121*, 1750.

(30) Meneses, A. B.; Antonello, S.; Arevalo, M. C.; Gonzalez, C. C.; Sharma, J.; Wallette, A. N.; Workentin, M. S.; Maran, F. *Chem.—Eur. J.* **2007**, *13*, 7983.
(31) Macias-Ruvalcaba, N. A.; Evans, D. H. *J. Phys. Chem. B* **2005**, *109*, 14642.
(32) Hong, S. H.; Kraiya, C.; Lehmann, M. W.; Evans, D. H. *Anal. Chem.* **2000**, *72*, 454.
(33) Rudolph, M. *J. Electroanal. Chem.* **2003**, *543*, 23.
(34) Te Velde, G.; Bickelhaupt, F. M.; Baerends, E. J.; Fonseca Guerra, C.; Van Gisbergen, S. J. A.; Snijders, J. G.; Ziegler, T. *J. Comput. Chem.* **2001**, *22*, 931.
(35) Guerra, C. F.; Snijders, J. G.; Te Velde, G.; Baerends, E. J. *Theor. Chem. Acc.* **1998**, *99*, 391.
(36) *ADF2013.01*; SCM, Theoretical Chemistry, Vrije Universiteit: Amsterdam, The Netherlands, 2013; http://www.scm.com.
(37) Perdew, J. P.; Burke, K.; Ernzerhof, M. *Phys. Rev. Lett.* **1996**, *77*, 3865.
(38) Grimme, S.; Ehrlich, S.; Goerigk, L. *J. Comput. Chem.* **2011**, *32*, 1456.
(39) van Lenthe, E.; Baerends, E. J.; Snijders, J. G. *J. Chem. Phys.* **1994**, *101*, 9783.
(40) Klamt, A. *J. Phys. Chem.* **1995**, *99*, 2224.
(41) de la Cruz, J. I.; Juarez-Saavedra, P.; Paz-Michel, B.; Leyva-Ramirez, M. A.; Rajapakshe, A.; Vannucci, A. K.; Lichtenberger, D. L.; Paz-Sandoval, M. A. *Organometallics* **2014**, *33*, 278.
(42) Humphrey, W.; Dalke, A.; Schulten, K. *J. Mol. Graphics* **1996**, *14*, 33.